Design and Characterization of a 250–350-GHz Fixed-Tuned Superconductor-Insulator-Superconductor Receiver

Cheuk-yu Edward Tong, *Member, IEEE*, Raymond Blundell, *Member, IEEE*, Scott Paine, *Member, IEEE*, D. Cosmo Papa, Jonathan Kawamura, Xiaolei Zhang, Jeffrey A. Stern, and Henry G. LeDuc

Abstract— **A fixed-tuned superconductor–insulator–superconductor (SIS) receiver has been designed to operate in the 250–350-GHz frequency band. This receiver has a double-side-band noise temperature of between 35 and 45 K, or about $3h\nu/k_B$, over its entire operating band. Extensive characterization of the receiver has been carried out using techniques developed for submillimeter waves. The input noise, side-band ratio, 1 dB compression point, optimum LO drive level, and vector near-field beam profile have all been measured experimentally. The measurement techniques and results are presented and discussed.**

I. Introduction

THE SUBMILLIMETER array (SMA), currently under construction by the Smithsonian Astrophysical Observatory, will function as a fully automated radio interferometer of six 6-m antennas. Fixed-tuned receivers incorporating superconductor–insulator–superconductor (SIS) mixers are being developed to cover the major submillimeter atmospheric windows [1]. The five target frequency bands are:

1) 176–256 GHz;
2) 250–350 GHz;
3) 400–520 GHz;
4) 600–720 GHz; and
5) 780–900 GHz.

The design and development of the receiver for the lowest SMA frequency band has been reported in a previous article [2]. This paper describes the work on the 250–350 GHz receiver. The emphasis of this paper is the experimental characterization of the receiver prototype. This incudes experimental measurements of noise temperature, losses incurred in front of the mixer element, side-band ratio, 1 dB compression point, local oscillator (LO) power level, and beam profile. Since test equipment working at submillimeter wavelengths is not readily available from commercial sources, different measurement techniques have been developed in house to allow a full characterization of the receiver. Some of these techniques are discussed in detail below, and experimental data is presented.

Manuscript received November 10, 1995; revised May 24, 1996.

C.-y. E. Tong, R. Blundell, S. Paine, D. C. Papa, J. Kawamura, and X. Zhang are with the Harvard-Smithsonian Center for Astrophysics, Cambridge, MA 02138 USA.

J. A. Stern and H. G. LeDuc are with the Center for Space Microelectronics Technology, Jet Propulsion Laboratory, Pasadena, CA 91109 USA.

Publisher Item Identifier S 0018-9480(96)06384-3.

II. Mixer Block Design

Fig. 1 is a detailed drawing of the central portion of the mixer block. The dimensions are essentially 70% of the corresponding dimensions of the 200 GHz mixer block from which the 300 GHz design is derived. The reduced height waveguide section (0.80×0.19 mm) is created by mechanical stamping. This shorted waveguide section, which forms the fixed backshort tuner of the mixer, measures 0.26 mm in depth. This mechanical layout, together with the low-pass IF filters, produces a driving point impedance of about 35 Ω at the waveguide feed point over the required operating bandwidth of 250–350 GHz [2].

The mixer block is fitted with an electroformed corrugated feed horn section that includes a transition from reduced height guide to corrugated guide. The semiflare angle of the horn is 8.5°. The fused quartz mixer chip, measuring $0.355 \times 0.090 \times 4$ mm, is clamped between the horn section and the mixer block back piece in a suspended microstrip line configuration, parallel to the E-plane of the waveguide. The chip is contacted on both the IF connector side and the ground side by gold plated beryllium copper wire, 0.125 mm in diameter. Since the contact pads on the chip are overlaid with a thin gold layer, no indium is needed to maintain the mechanical contact. Two grooves are milled on each side of the block along the H-plane of the waveguide. They allow a pair of magnetic pole pieces to come into close proximity of the SIS junction.

III. Junction Design and Tuning

At the center of the mixer chip is the waveguide to thin-film microstrip transition. A thin-film microstrip coupling network has been designed to couple the junction to the driving point impedance of 35 Ω provided by the waveguide circuitry.

The ground plane of the thin-film microstrip line is the 150 nm thick base electrode of the SIS junction trilayer, while the microstrip line is the 230-nm-thick wiring layer of the junction. The insulator is simply the 200 nm layer of SiO used to electrically isolate the Nb/AlO_x/Nb junction [3]. Since the frequency involved is below half the gap frequency of niobium (f_g(Nb) = 700 GHz), a two fluid model is used in the design process. The penetration depth, λ_L, is taken as 75 nm. The slow wave factor, $\sqrt{\varepsilon_{\text{line}}}$, and the characteristic impedance, Z_{line}, of the superconducting microstrip line are derived from

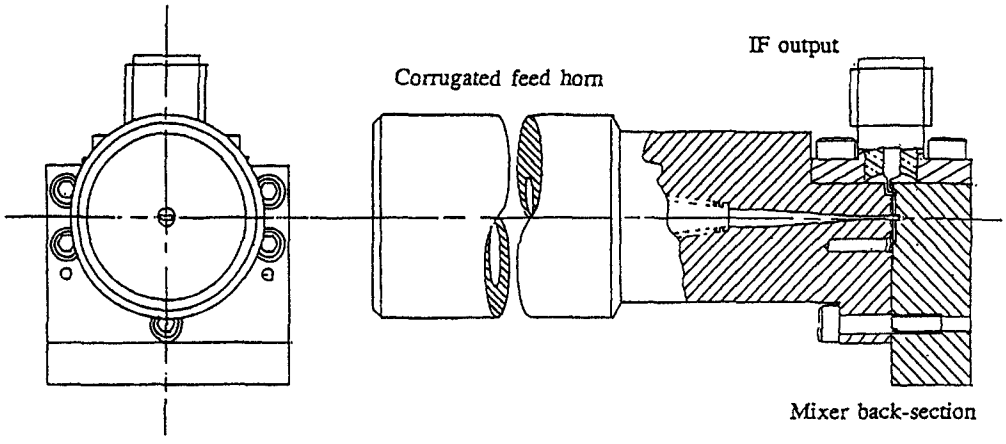

(a)

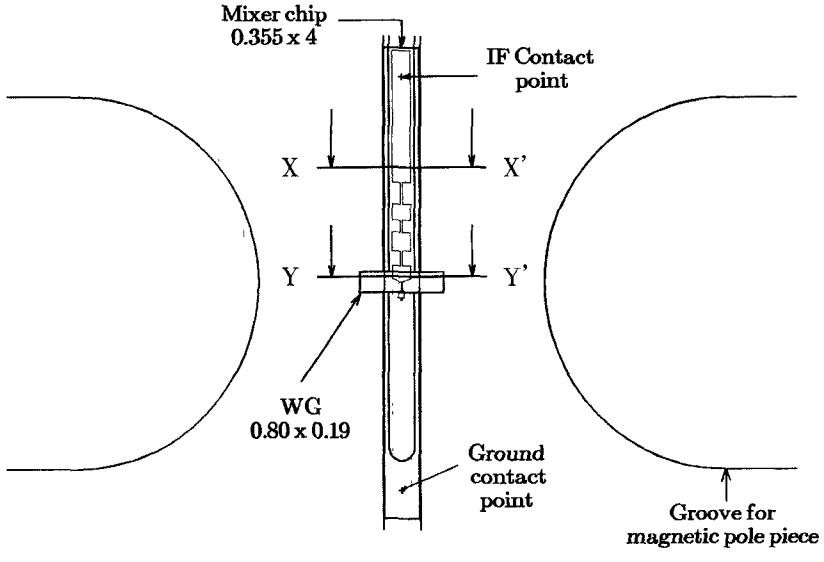

(b)

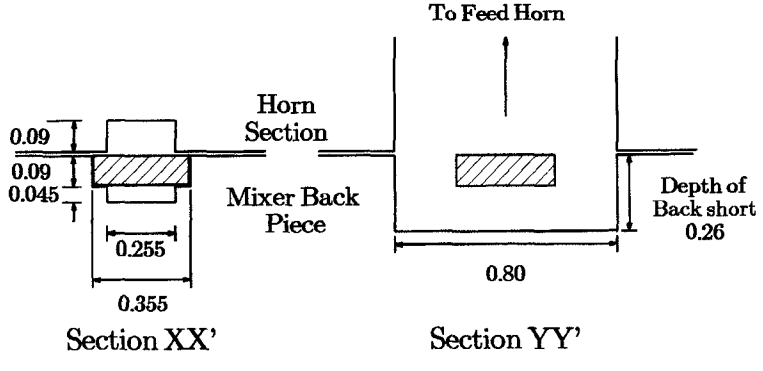

(c)

Fig. 1. (a) Mixer mount detail showing the corrugated horn section and the mixer back piece. (b) View of the mixer back piece from the side of the horn. The mixer chip sits in a channel along the E-plane of the waveguide. (c) Sectional views of the mixer back piece. The quartz substrate is hatched. Section XX′ shows the cross section of the suspended strip line low-pass filter. Section YY′ shows the fixed back short of the mixer. All dimensions are in mm.

incremental inductance considerations [4]

$$Z_{\text{line}} = SZ_p \qquad \text{and} \qquad \sqrt{\varepsilon_{\text{line}}} = S\sqrt{\varepsilon_p} \tag{1}$$

where Z_p is the characteristic impedance, ε_p is the effective dielectric constant of the perfectly conducting microstrip line with the same geometry, and S is a scaling factor derived in the Appendix. Using these simple closed-form expressions, a coupling network consisting of a two section transformer plus a short inductive line has been designed with the aid of a commercial linear RF package.

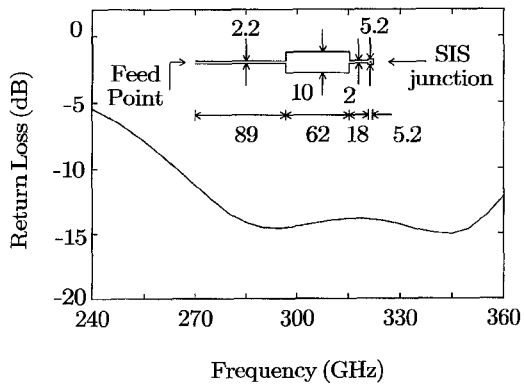

Fig. 2. Layout and theoretical return loss of the coupling network to the SIS junction. All dimensions are in μm. The return loss is the match seen at the waveguide feed point to a 35 Ω source impedance.

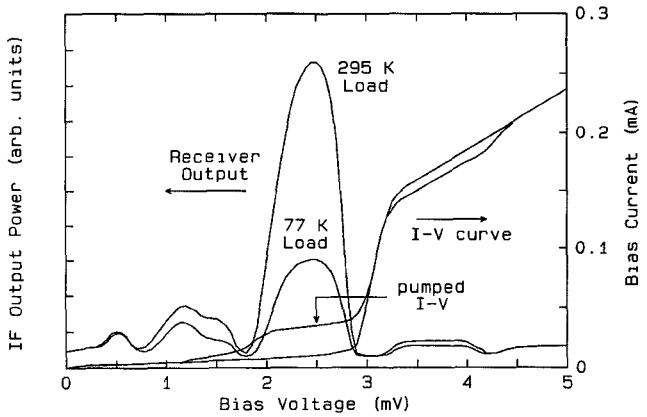

Fig. 3. IF output power of the receiver as a function of bias voltage in a hot/cold load measurement. The LO frequency is 270 GHz. Also shown is the current-voltage characteristics (I-V) of the SIS device with and without LO power. Two point measurement has been used and the series resistance involved is about 2 Ω. Note that at a bias voltage of 2.5 mV, a Y-factor of 2.86 is obtained.

Reproducibility and tolerance considerations dictate a minimum line width of 2 μm. This implies a maximum characteristic impedance of about 16 Ω. We have, therefore, chosen a target source impedance at the junction to be 15 Ω. Using the results of computer simulations [5], [6], we establish that the target normal state resistance, R_N, is 20 Ω.

The percentage bandwidth of the coupling network is determined by the ωCR product of the junction, which in turn is dictated by the critical current density of the junction, J_c. In order to cover the 33% bandwidth, centered about 300 GHz, the maximum allowable value of ωCR is 3 [7]. With $R_N = 20\ \Omega$, the required junction capacitance is thus 80 fF. Assuming a specific junction capacitance of 65 fF/μm^2, the junction size, A, is 1.1 μm $\times$ 1.1 μm. Since $J_c R_N A = 1.9$ mV for niobium tunnel junctions, the required J_c is therefore 8 kA/cm^2.

Since the IF of the SMA is 5 GHz, which is significantly higher than the more popular 1.5 GHz IF of most SIS receivers, it is important to minimize the IF output capacitance introduced by the coupling network. Consequently, instead of having a quarter-wave low impedance section, we have used a low impedance section with an electrical length of only 70°. Even in this configuration this section still makes up about half of the total IF output capacitance, which is about 0.3 pF. This is equivalent to a reactance of 100 Ω at 5 GHz.

The layout of the integrated tuner and predicted return loss are given in Fig. 2. Note that the center frequency of the design is shifted toward the higher end of the target frequency band. This is because the receiver is required to have good performance at 345 GHz, an astrophysically important frequency.

IV. Receiver Noise Measurement

The mixer block is installed in a liquid helium cryostat for laboratory noise temperature measurements. The vacuum window is a 0.66-mm-thick Teflon sheet. This is followed by an infrared block, a thin porous Teflon sheet mounted on the radiation shield. A grooved lens, mounted on the cold plate, focuses the incoming beam onto the corrugated feed. Double-side-band (DSB) receiver noise temperatures are measured using the standard hot (295 K) and cold (77 K) load method. Linear noise temperatures are computed from the experimental Y-factor without any corrections for losses in the input optics. The IF amplifier has a noise temperature of about 8 K. Measurements are made with a 1 GHz IF bandwidth, centered at 5 GHz. LO power is injected either through a dielectric beam-splitter that has an insertion loss of about 1%, or through a polarizing wire grid.

Fig. 3 shows the current-voltage characteristics of a typical SIS mixer with and without LO power, as well as the receiver output power as a function of bias in response to hot and cold input loads. The R_N of this particular SIS junction is about 18 Ω, and the ratio of its subgap leakage resistance, R_{sg}, to R_N is about 15, at a physical temperature of 4.2 K. The critical current density is 8.2 kA/cm^2 and the area of the junction is about 1.35 μm^2. From the figure, a Y-factor of 2.86 is obtained, corresponding to a DSB receiver noise temperature of 40 K.

The measured receiver noise temperature is plotted against LO frequency in Fig. 4. The noise temperature is reasonably flat, equivalent to about $3h\nu/k_B$ over the target frequency band. The noise performance of the receiver seems to be a few Kelvin better with the dielectric beam-splitter. This suggests that the cross-polarization loss due to the mixer feed and lens is about 2%. A number of other SIS mixer chips of the same design have been tested in the same mixer block and have shown comparable performance.

V. Analysis of Noise Contributions

The measured receiver noise temperature can be broken down into three components:

1) input noise, $T_{\rm inp}$, or noise introduced in front of the mixer element;
2) mixer noise, T_m; and
3) multiplied IF amplifier noise, $L_c T_{\rm IF}$.

Since an isolator is used in front of the first IF amplifier, the determination of the last component is relatively straight forward, once the IF system has been characterized [8], [9].

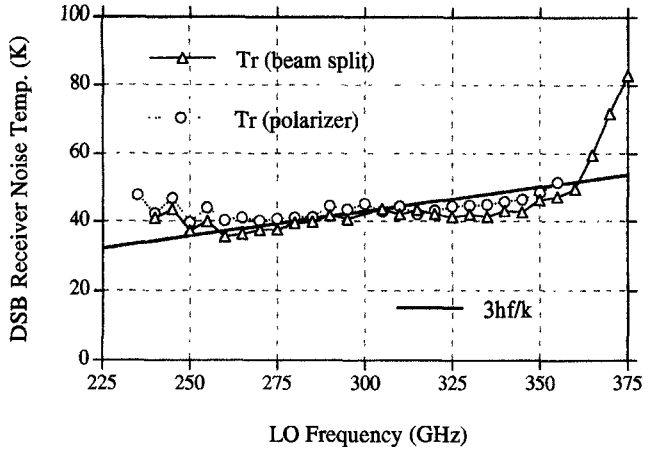

Fig. 4. Double-side-band receiver noise temperature as a function of LO frequency when the LO injector is a dielectric beam-splitter (△) and a wire grid polarizer (○). Also shown, is the line $T_{\text{noise}} = 3h\nu/k_B$.

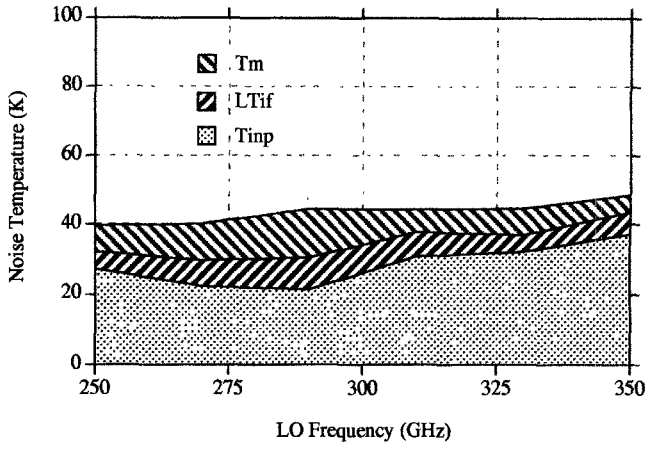

Fig. 6. Breakdown of the measured noise temperature into input noise, T_{inp}; multiplied IF noise $L_c T_{\text{IF}}$; and mixer noise, T_m. In these measurements, a wire grid polarizer is used as LO injector.

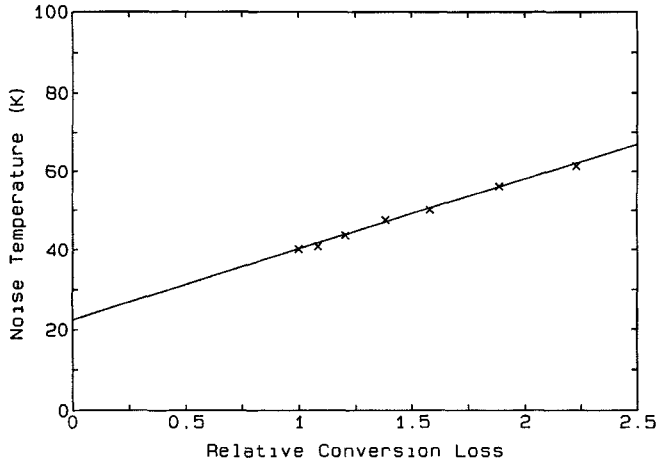

Fig. 5. Receiver noise temperature at different LO power levels plotted against relative conversion loss. The LO frequency is 270 GHz and the LO injector is a wire grid. Conversion loss is normalized to the optimum value obtained under the operating condition in Fig. 4. The fitted line cuts the vertical axis at an intercept of 22 ± 2 K.

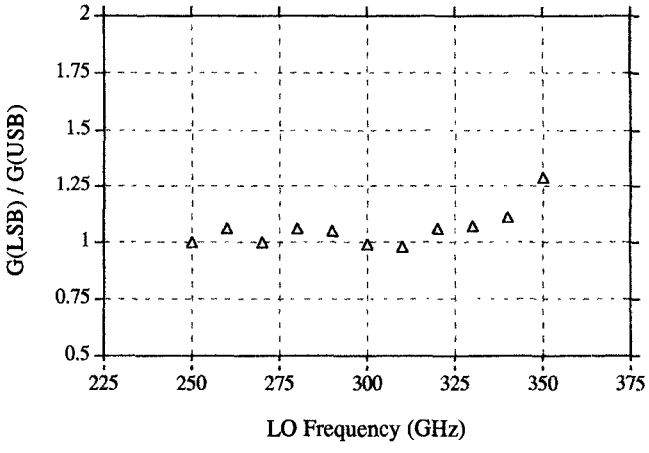

Fig. 7. Side-band ratio, $G_{\text{LSB}}/G_{\text{USB}}$, as a function of LO frequency.

Input noise can be determined by the method of "intersecting lines" [10], [11]. In this method, the junction is biased at a fixed voltage and hot/cold load measurements are repeated for a number of different LO power levels below the optimal level. We can plot receiver noise temperature against relative conversion loss, which is inversely proportional to the difference between the receiver outputs in the hot/cold load measurements. An example of such a data set is given in Fig. 5. It can be seen that the data points fall onto a straight line. The intercept of this line on the vertical axis represents the noise temperature component that is independent of the conversion efficiency of the mixer. It has been demonstrated that the SIS mixer output noise is a constant, so that T_m has a linear dependence on mixer conversion loss [12]. Consequently, the value of the intercept is T_{inp}. From the figure, we determine that at an LO frequency of 270 GHz, T_{inp} is 22 ± 2 K.

Using the above experimental procedures, we have been able to separate the measured receiver noise temperature into its three components. The results are presented in Fig. 6. The largest component is the input noise, which is about 20 K at the center of the band and rises to 37 K at 350 GHz. This suggests an input coupling loss of 6 to 12%, assuming that the losses occur at room temperature. The wire grid injector accounts for about 3% of the loss. The remaining loss can be attributed to imperfection in the cold load; absorption and scattering of the beam by the lens and windows; as well as wide angle side lobes of the horn.

VI. Side-Band Ratio Measurement

The two side-bands of the mixer are separated by 10 GHz, which is about 3% of the center frequency of the input band. Since the mixer maintains low-noise performance over a bandwidth in excess of 100 GHz (or 33% of the center frequency), there should be little doubt that the side-bands are equally down converted to the IF band. Nevertheless, it is desirable to quantify the balance of the side-bands, $G_{\text{LSB}}/G_{\text{USB}}$ because intensity calibration of an observed spectral line depends on this ratio.

In order to measure the side-band ratio, we have used a Martin-Puplett Interferometer (MPI) as a single-side-band filter [13]. A technique has been employed whereby only one

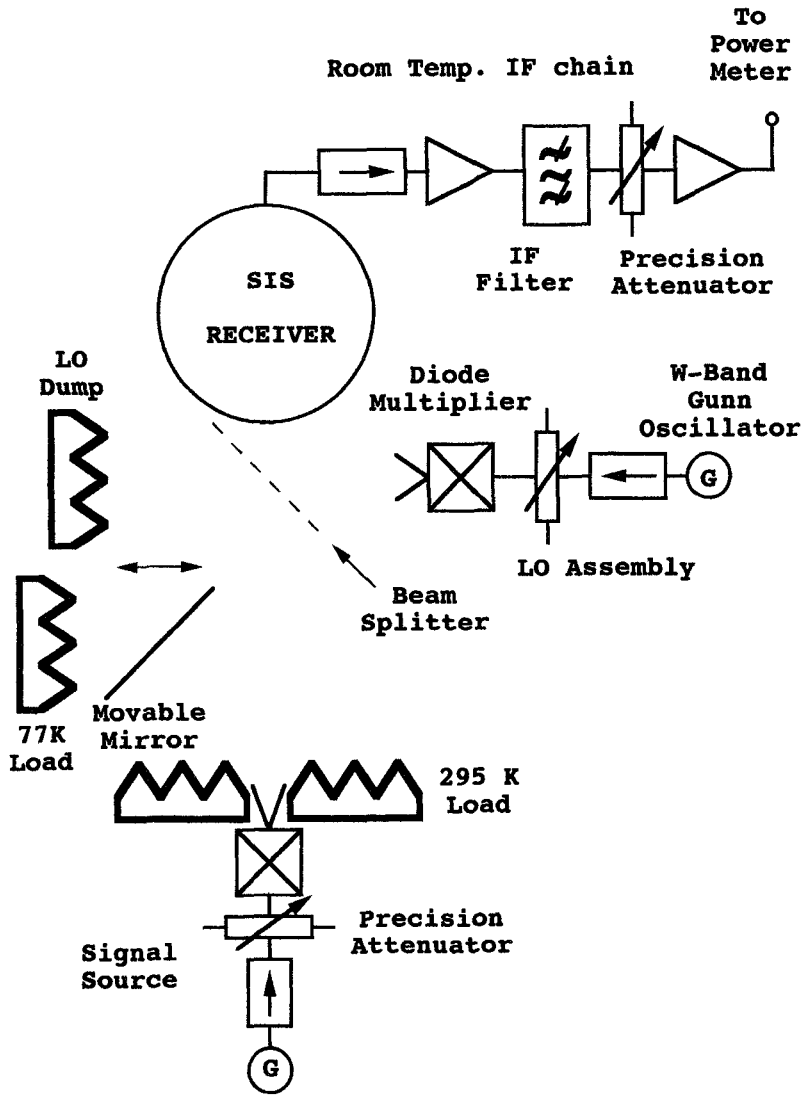

Fig. 8. Measurement setup for P_{1dB} and incident LO power. The movable mirror can be inserted into the signal beam to allow a cold load measurement. The signal source is placed sufficiently far from the receiver so that the aperture of its horn is small when compared to the beam size.

fixed oscillator is needed to perform the measurement. The LO assembly is fixed at one port of the MPI and the other port faces the hot/cold loads. We first set the LO to the upper-side-band frequency. The MPI is tuned to reject this frequency by using the SIS junction as a direct detector. This procedure is repeated for the lower-side-band. The best rejection positions for both cases are noted. Next, we rotate the analyzer grid of the MPI by 90 degrees. The polarization of the LO beam is also rotated by 90 degrees by inserting a waveguide twist. Hot/cold load measurements are performed successively at the signal port when the MPI is tuned to act as an upper-side-band and lower-side-band rejection filter. Care is taken so that the measurements are made with the same detected current flowing in the voltage-biased junction. The side-band ratio is simply the ratio of the conversion losses. The side-band ratio can be measured to an accuracy of about 0.05, ensuring that the calibration uncertainty of spectral lines due to side-band ratio error is less than 2.5%.

The measured ratio is plotted against LO frequency in Fig. 7. This value is close to unity from 250 GHz to 330 GHz, and rises to about 1.3 at 350 GHz. This measurement confirms that the receiver operates in the DSB mode.

VII. Saturation and LO Power Measurement

SIS radiometers are most often used to measure very small signals so that saturation resulting from too high a level of input signal should not exist. However, there has been some concern that broadband mixers may saturate [14], [15]. Since saturation may affect the linearity of the mixer, gain calibration made with hot and cold loads may not be accurate. At lower frequencies, saturation measurements of SIS mixers using CW and broad-band noise sources have been performed using waveguide inputs [16]. We have devised a scheme for measuring the linearity of the mixer in the presence of a quasioptically coupled CW signal.

Referring to Fig. 8, this measurement requires two submillimeter sources, one as the LO and one as the signal. The signal source can be two orders of magnitude weaker than the LO. However, it is easier for calibration purposes to employ a

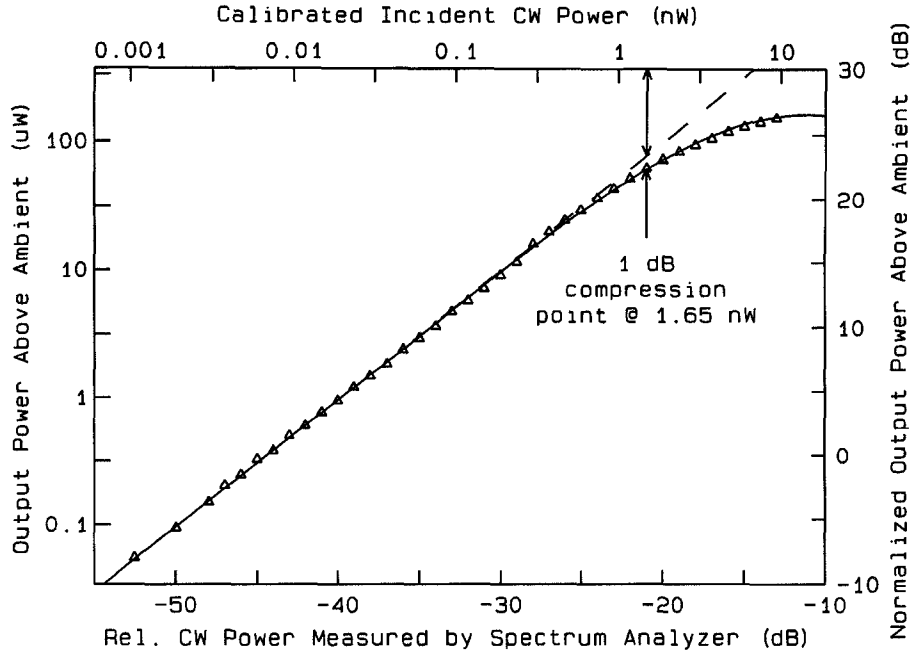

Fig. 9. Gain compression characteristics of the receiver. The measurement frequency is 270 GHz. On the y-axis, the left scale is $P_{\rm out} - P_{\rm hot}$ in μW (log scale) while the right scale is $(P_{\rm out} - P_{\rm hot})/(P_{\rm hot} - P_{\rm cold})$ in dB. On the x-axis, the lower scale represents the IF power (in dBm) measured by the harmonic mixer/spectrum analyzer while the upper scale is the incident CW power in nW as calibrated by (2). The solid line is the best fit polynomial to the measured data ($\triangle$) and the dotted line is the unity slope tangent.

source of comparable strength and to simply place the signal source at a larger distance from the receiver. First, a hot/cold load measurement is performed with no added signal. Let $P_{\rm hot}$ and $P_{\rm cold}$ be the corresponding receiver output powers. Next, the receiver output power, $P_{\rm out}$, is measured at different incident signal levels over an ambient background. The signal level is set by the precision variable attenuator in the signal source chain. Note that a coaxial precision variable attenuator is inserted in the IF chain to prevent saturation of its last stage. The relative incident signal power, $P_{\rm rel}$, is then measured with a spectrum analyzer by connecting a waveguide harmonic mixer directly to the signal source. By plotting $P_{\rm out} - P_{\rm hot}$ against $P_{\rm rel}$, we can determine the range of $P_{\rm out}$ over which the receiver is linear.

Absolute calibration of the incident CW signal power is made using the values $P_{\rm hot}$ and $P_{\rm cold}$. Over the linear regime of the receiver

$$P_{\rm CW} = 2k_{\rm B}B_m\Delta T\frac{P_{\rm out} - P_{\rm hot}}{P_{\rm hot} - P_{\rm cold}} \qquad (2)$$

where $\Delta T = (295 - 77)$ K and B_m is the noise equivalent bandwidth of the receiver at the input of the power meter that measures $P_{\rm out}$. The factor of 2 in (2) comes from the assumption of a unity side-band ratio.

A set of data measured at around 270 GHz is displayed in Fig. 9, from which the 1 dB input CW compression power, $P_{1\,\rm dB}$, is determined to be 1.65 nW above the ambient background. In an SIS mixer, gain compression is caused by saturation at the IF output port [17], [18]. Therefore, the amount of incident RF power from the ambient background contributing to gain compression is $2k_BT_{\rm amb}B_t$, where B_t is the noise equivalent output bandwidth of the mixer [15]. Considering this background incident power together with the uncertainty in side-band ratio and other experimental uncertainties, we conclude that $P_{1\rm dB}$ is $1.7(\pm 0.2)$ nW.

Following the approach in [17], the theoretical input compression power can be determined from the variation of conversion gain with bias voltage about the dc bias point. Using the data from Fig. 3, we establish that for an IF output of $V_{\rm IF}\sin\omega_{\rm IF}t$, the time-averaged conversion gain is

$$G(V_{\rm IF}) = G(0)\left[1 - 2.412V_{\rm IF}^2 + 0.975V_{\rm IF}^4\right] \qquad (3)$$

where $V_{\rm IF}$ is in mV. The 1 dB output compression point occurs when $V_{\rm IF} \sim 0.3$ mV. The SSB conversion loss is $-2(\pm 1)$ dB and the IF load resistance is 50 Ω. Therefore, we deduce that the input compression power is $1.4(\pm 0.3)$ nW, in good agreement with our experimental data. This result suggests that the receiver is still highly linear when subjected to radiation from an ambient load.

By extrapolating the above calibration for incident CW power, we can use the same scheme to measure the LO drive level at the input of the receiver. In this case the LO is turned off and power from the signal source is increased until the SIS junction is pumped to the same level as by the LO assembly. Using this procedure, we determine that the optimum LO drive is $38.3(\pm 0.2)$ dB above $2k_BB_m\Delta T$, which is equivalent to $50(\pm 8)$ nW.

VIII. Beam Profile

The optical system in the SMA is of an imaging design [19]. The aperture of the receiver feed horn is imaged onto the secondary mirror of the telescope by a lens and by a pair of focusing mirrors common to all receivers. To verify the design of the horn-lens combination, near field measurements of the emerging beam profile have been made.

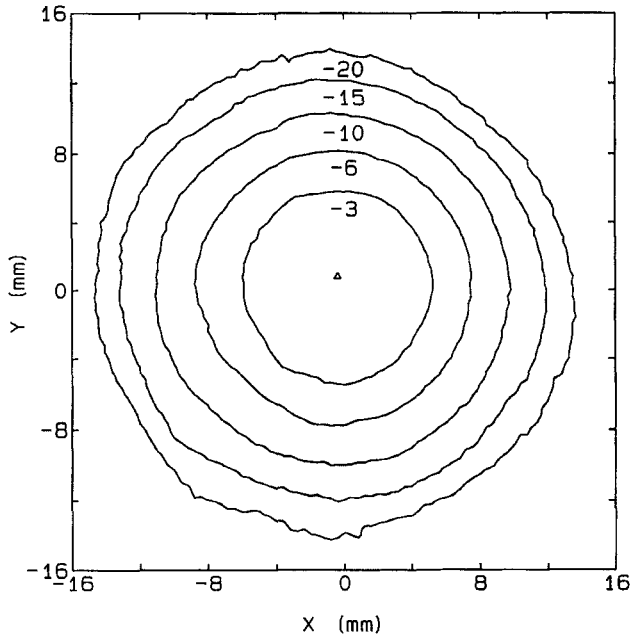

Fig. 10. Two-dimensional (2-D) amplitude pattern of the receiver at a signal frequency of 298.8 GHz. The H-plane of the feed is along the x-axis and the E-plane is along the y-axis. Contours at -3, -6, 10, -15 and -20 dB are plotted.

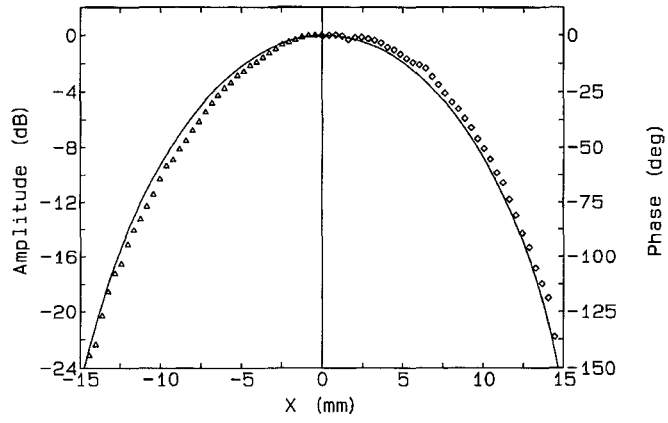

Fig. 11. Comparison between the measured and theoretical beam patterns in the H-plane. The solid line is the theoretical profile. The data on the left hand side is the amplitude in dB and that on the right hand side is the phase in degrees. Measured data points are indicated by ($\triangle$) for amplitude and by ($\diamond$) for phase.

The details of the vector near-field antenna measurement system have been reported elsewhere [20], [21]. In this case, the transmitter probe is a WR-3 open waveguide. This is scanned in a plane 219 mm from the lens. The transmitted power is of the order of 100 pW. Estimating the coupling loss between the probe and the receiver to be about 30 dB, the receiver is operating well below the saturation level. The dynamic range of the measurement is about 32 dB. The maximum RMS phase error introduced by the flexible cable connecting the scanning transmitter is estimated to be about 5 degrees.

Fig. 10 gives the measured amplitude pattern at a signal frequency of 298.8 GHz. The scan consists of 81×81 points spaced 0.4 mm apart and the total scan time is about 40 min. At the -15 dB points, the beam is 25 mm wide in the H-plane and is 24 mm wide in the E-plane. No side lobes are observed down to the -25 dB level. In Fig. 11, the measured amplitude and phase in the H-plane are compared to the designed near-field values. The agreement is very good, the RMS deviation of the measured phase profile from the theoretical profile being about 1 degree. The agreement indicates that the horn-lens spacing and lens focal length are together accurate to within about 2%. Note that the phase of the beam at the scan plane is essentially flat—the radius of curvature of the phase front is about 9.4 m, much bigger than the -10 dB full beam-width of 20 mm. Given that the beam is very slow, no probe correction is needed.

IX. Heterodyne Testing

Upon the completion of the SMA telescopes, SIS receivers will be used to measure spectra of different molecules in the interstellar medium. In order to simulate the real working mode of operation, we have coupled the receiver output beam to a 50 cm long gas cell filled with methanol vapor, maintained at a pressure of 0.025 mbar. In this measurement, the receiver views a 77 K cold load through the gas cell, which is at room temperature.

Fig. 12 shows the emission spectrum of methanol at a frequency of 250.507 GHz [22]. At the spectral line transition, the gas is still optically thin. The system noise temperature measured through the gas cell is 146 K. This includes a signal coupling loss of about 30% due to absorption and reflections from the thick Teflon vacuum windows of the gas cell. The random variation of the baseline of the spectrum is about 0.7 K, corresponding to a signal-to-noise ratio (SNR) of 10. This SNR is obtained by averaging 40 readings from a power meter, with a resolution bandwidth of 100 kHz. The measured full width at half maximum of the spectral line of 900 kHz agrees well with the theoretical Doppler width at the pressure of the gas. This experiment confirms that this SIS receiver can be used as a powerful tool to measure emission spectra of molecules.

X. Conclusion

A fixed-tuned SIS receiver incorporating a mixer with an integrated tuner has been designed to cover the frequency band 250–350 GHz. The noise temperature of this receiver is flat and remains close to $3h\nu/k_B$ over the entire frequency band. Different techniques have been developed to characterize its performance. These include the separation of receiver noise into its constituent parts, measurement of side-band ratio, input compression power, required LO drive and near-field beam profile. All these rigorous tests confirm that this receiver will be a valuable instrument for astronomical observations at 1 mm wavelength.

Appendix

For a superconducting microstrip transmission line, the series impedance and shunt admittance, per unit length, can

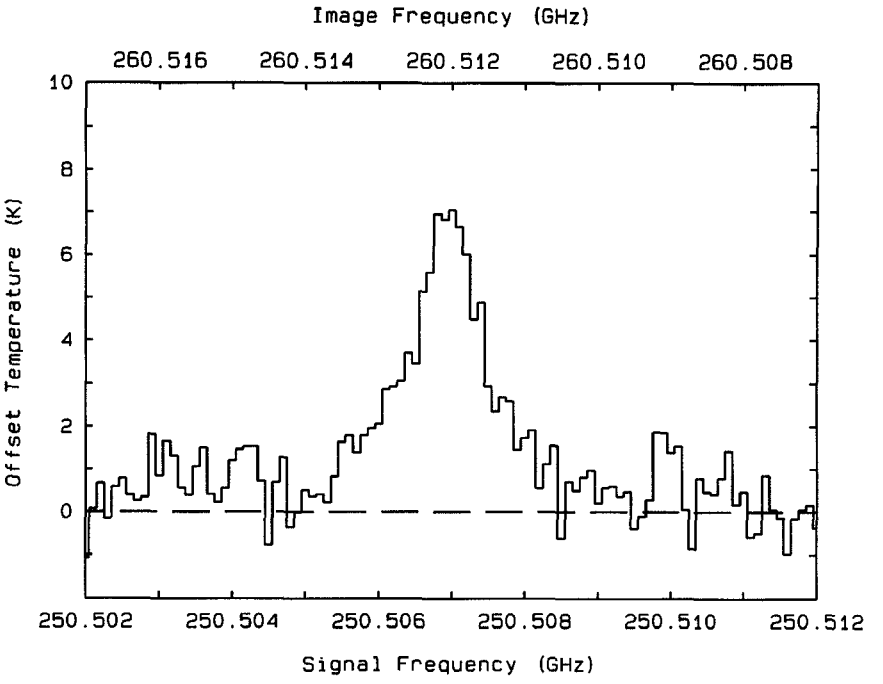

Fig. 12. Emission spectrum of methanol vapor at 0.025 mbar at 258.507 GHz. The LO frequency is 255.5095 GHz and the spectral resolution bandwidth is 100 kHz. The vertical scale is the line intensity (in K) above the 77 K cold load background.

be written as [23]

$$Z = j\omega\mu_0 g_1 + 2g_2 Z_s \tag{4}$$

$$Y = j\omega\varepsilon_0\varepsilon_p / g_1 \tag{5}$$

where g_1 and g_2 are geometrical factors, ε_p is the effective dielectric constant of the corresponding perfectly conducting microstrip line and Z_s is the surface impedance. Here we assume that the loss of the dielectric is negligible. The characteristic impedance and propagation constant of this superconducting transmission line are

$$Z_{\text{line}} = \sqrt{\frac{Z}{Y}} = \frac{g_1\eta_0}{\sqrt{\varepsilon_p}}\sqrt{1 - j\frac{2g_2 Z_s}{\omega\varepsilon_0 g_1\eta_0^2}} \tag{6}$$

$$\gamma = \sqrt{ZY} = jk_0\sqrt{\varepsilon_p}\sqrt{1 - j\frac{2g_2 Z_s}{\omega\mu_0 g_1}} \tag{7}$$

where η_0 is the free space impedance. For the corresponding perfectly conducting line, $Z_s = 0$. Its characteristic impedance is

$$Z_p = g_1\eta_0/\sqrt{\varepsilon_p}. \tag{8}$$

At frequencies below the gap, the loss of the line is of the order of 0.1 dB/λ_g [24] and can, therefore, be neglected. Assuming also that both the strip and the ground plane are thick compared to the penetration depth, we can write, using the two fluid model [25]

$$Z_s = j\omega\mu_0\lambda_L. \tag{9}$$

Applying the (8) and (9) to (6) and (7), we obtain

$$Z_{\text{line}} = SZ_p \quad \text{and} \quad \gamma = jSk_0\sqrt{\varepsilon_p} \tag{10}$$

where

$$S = \sqrt{1 + \frac{2g_2\eta_0}{Z_p\sqrt{\varepsilon_p}}\lambda_L} \tag{11}$$

η_0 being the free space impedance. Closed form analytical expression for g_2 is given in [4].

ACKNOWLEDGMENT

The authors would like to thank M. Smith for his superior technical assistance, M.-t. Chen of ASIAA, Taiwan, for his assistance in some of the measurements and K. Wu of Ecole Polytechnique, Montréal, for discussions on propagation characteristics of superconducting transmission lines.

REFERENCES

[1] T. G. Phillips and J. Keene, "Submillimeter astronomy," *Proc. IEEE*, 1992, vol. 80, pp. 1662–1701.
[2] R. Blundell, C. E. Tong, D. C. Papa, R. L. Leombruno, X. Zhang, S. Paine, J. A. Stern, and H. G. LeDuc, "A wideband fixed-tuned SIS receiver for 200 GHz operation," *IEEE Trans. Microwave Theory Tech.*, vol. 43, pp. 933–937, 1995.
[3] H. G. LeDuc, J. A. Stern, S. Thakoor, and S. Khanna, "All refractory NbN/MgO/NbN SIS tunnel junctions," *IEEE Trans. Magn.*, vol. MAG-23, pp. 863–865, 1987.
[4] R. A. Pucel, D. J. Massé, and C. P. Hartwig, "Losses in microstrip," *IEEE Trans. Microwave Theory Tech.*, vol. MTT-16, pp. 342–350, 1968: see also correction in vol. MTT-16, p. 1064, 1968.
[5] C. E. Tong and R. Blundell, "Simulation of the superconducting quasiparticle mixer using a five-port model," *IEEE Trans. Microwave Theory Tech.*, vol. 38, pp. 1391–1398, 1990.
[6] Q. Ke and M. Feldman, "Optimum source conductance for high frequency superconducting quasiparticle receivers," *IEEE Trans. Microwave Theory Tech.*, vol. 41, pp. 600–604, 1993.
[7] A. R. Kerr, "Some fundamental and practical limits on broadband matching to capacitive devices, and the implications for SIS mixer design," *IEEE Trans. Microwave Theory Tech.*, vol. 43, pp. 2–13, 1995.
[8] D. P. Woody, "Measurement of the noise contribution to SIS heterodyne receivers," *IEEE Trans. Appl. Supercond.*, vol. 5, pp. 3312–3315, 1995.

[9] M. W. Pospieszalski, "On the noise parameters of isolator and receiver with isolator at the input," *IEEE Trans. Microwave Theory Tech.*, vol. MTT-34, pp. 451–453, 1986: see also correction in vol. MTT-34, p. 746, 1986.
[10] R. Blundell, R. E. Miller, and K. H. Gundlach, "Understanding noise in SIS receivers," *Int. J. IR & MM Waves*, vol. 13, pp. 3–16, 1992.
[11] Q. Ke and M. J. Feldman, "A technique for noise measurements of SIS receivers," *IEEE Trans. Microwave Theory Tech.*, vol. 42, pp. 752–755, 1994.
[12] ——, "Constant output noise temperature of the superconducting quasiparticle mixer," *IEEE Appl. Supercond.*, vol. 3, pp. 2245–2249, 1993.
[13] J. C. G. Lesurf, *Millimeter-Wave Optics, Devices and Systems.* Bristol and New York: Adam Hilger, 1990.
[14] M. J. Feldman and L. R. D'Addario, "Saturation of the SIS detector and the SIS mixer," *IEEE Trans. Magn.*, vol. MAG-23, pp. 1254–1258, 1987.
[15] L. R. D'Addario, "Saturation of the SIS mixer by out-of-band signals," *IEEE Trans. Microwave Theory Tech.*, vol. 36, pp. 1103–1105, 1988.
[16] S. K. Pan, A. R. Kerr, M. J. Feldman, A. W. Kleinsasser, J. W. Stasiak, R. L. Sandstrom, and W. J. Gallagher, "An 85–116 GHz SIS receiver using inductively shunted edge junctions," *IEEE Trans. Microwave Theory Tech.*, vol. 37, pp. 580–591, 1989.
[17] A. D. Smith and P. L. Richards, "Analytic solutions to superconductor-insulator-superconductor quantum mixer theory," *J. Appl. Phys.*, vol. 53, pp. 3806–3812, 1982.
[18] J. R. Tucker and M. J. Feldman, "Quantum detection at millimeter wavelengths," *Rev. Mod. Phys.*, vol. 57, pp. 1055–1113, 1985.
[19] S. Paine, D. C. Papa, R. L. Leombruno, X. Zhang, and R. Blundell, "Beam waveguide and receiver optics for the SMA," in *Proc. 5th Int. Symp. Space THz Tech.*, Ann Arbor, MI, May 1994, pp. 811–823.
[20] C. E. Tong, S. Paine, and R. Blundell, "Near-field characterization of 2-D beam patterns of submillimeter superconducting receivers," in *Proc. 5th Int. Symp. Space THz Tech.*, Ann Arbor, MI, May 1994, pp. 660–673.
[21] C. E. Tong, R. Blundell, and Y. Uzawa, "Near-field probing the beam profile of superconducting receivers in the 200 GHz frequency range," *IEEE Ant. & Propagat. Soc. Int. Symp.*, Seattle, WA, pp. 552–555, June 1994.
[22] F. J. Lovas, "Recommended rest frequencies for observed interstellar molecular microwave transitions—1991 revision," *J. Phys. Chem. Ref. Data*, vol. 21, pp. 181–280, 1992.
[23] K. C. Gupta, R. Garg, and I. J. Bahl, *Microstrip Lines and Slotlines.* Dedham, MA: Artech House, 1979.
[24] C. E. Tong and K. Wu, "Propagation characteristics of thin film superconducting microstrip line for terahertz applications," *Electron. Lett.*, vol. 27, pp. 2299–2300, 1991.
[25] T. Van Duzer and C. W. Turner, *Principles of Superconductive Devices and Circuits.* New York: Elsevier, 1980.

Cheuk-yu Edward Tong (M'89), for a photograph and biography, see p. 388 of the March 1994 issue of this TRANSACTIONS

Raymond Blundell (M'91), for a photograph and biography, see p. 388 of the March 1994 issue of this TRANSACTIONS

Scott Paine (M'93), for a photograph and biography, see p. 937 of the April 1995 issue of this TRANSACTIONS.

D. Cosmo Papa, for a photograph and biography, see p. 937 of the April 1995 issue of this TRANSACTIONS.

Jonathan Kawamura graduated from the California Institute of Technology, Pasadena, in 1992 and is currently pursuing graduate studies in the Department of Astronomy at Harvard University, Cambridge, MA.

Xiaolei Zhang, for a photograph and biography, see p. 1274 of the August 1993 issue of this TRANSACTIONS

Jeffrey A. Stern, for a photograph and biography, see p. 706 of the April 1994 issue of this TRANSACTIONS.

Henry G. LeDuc, for a photograph and biography, see p. 706 of the April 1994 issue of this TRANSACTIONS